

## A Switchable Surface Enables Detection of Single DNA Hybridization Events with Atomic Force Microscopy

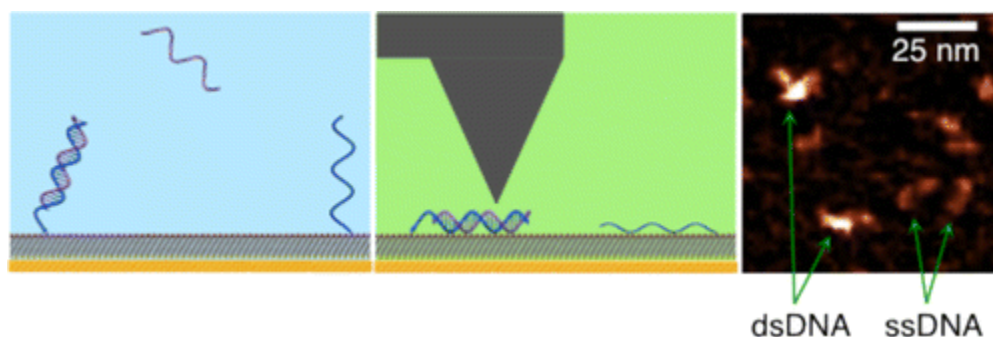
By: Gary R. Abel, Jr., [Eric A. Josephs](#), Norman Luong, and Tao Ye

Abel, Jr., G. A., Josephs, E. A., Luong, N., Ye, T. "A Switchable Surface Enables Detection of Single DNA Hybridization Events with Atomic Force Microscopy." *Journal of the American Chemical Society*, **2013**, 135 (17), 6399–6402. <https://doi.org/10.1021/ja401036t>

**This document is the Accepted Manuscript version of a Published Work that appeared in final form in *Journal of the American Chemical Society*, copyright © American Chemical Society after peer review and technical editing by the publisher. To access the final edited and published work see <https://doi.org/10.1021/ja401036t>.**

### Abstract:

Here we describe a novel surface that enables direct visualization of the hybridization of single DNA molecules with an unprecedented resolution using atomic force microscopy. The surface consists of single-stranded DNA probes that are covalently anchored to a self-assembled monolayer. The surface satisfies the contradictory requirements for high-resolution imaging and hybridization by switching the DNA-surface interaction between a strong state and a weak state. Our approach opens up unique opportunities in elucidating hybridization at the molecular scale.



**Keywords:** DNA | hybridization | atomic force microscopy

### Article:

The hybridization between DNA molecules immobilized on a solid support and complementary nucleic acid targets underlies a wide spectrum of nucleic acid sensors and microarray technologies.<sup>(1-6)</sup> The affinity, selectivity, and kinetics of surface hybridization are profoundly impacted by the nanoscale arrangement of immobilized DNA molecules (probes) on the sensor/microarray surfaces.<sup>(1, 3-5)</sup> As the interprobe interactions become significant when the probes are separated by  $<10$  nm<sup>(5)</sup> and the heterogeneity on sensor surfaces makes it difficult to interpret results from ensemble measurements, a critical bottleneck in understanding and optimizing the capture of complementary nucleic acids (targets) through hybridization is the lack of tools that can visualize hybridization at the sub-10 nm scale and single-molecule level. Although atomic force microscopy (AFM) would seem an ideal technique to address this issue,

single-molecule AFM imaging of DNA is mostly limited to nucleic acids immobilized on mica.<sup>(7-9)</sup> While such studies provided valuable insights into the conformations of DNA,<sup>(7-9)</sup> they are of limited relevance to surface hybridization as the targets and probes experience local interactions that are very different from those on mica. The nanoscale visualization of hybridization reactions has proven to be significantly more challenging,<sup>(10-16)</sup> owing to an apparent paradox:<sup>(4,17)</sup> To achieve a high AFM imaging resolution, the biomolecule must be strongly bound to the surface and remain stationary as the tip traverses over the molecule; however, to allow for hybridization or other reactions, the surface must be passivated with inert molecules that reduce the nonspecific interactions with the biomolecules.<sup>(18)</sup> Due to the rapid fluctuation of surface-anchored DNA probes,<sup>(11, 16, 19)</sup> most AFM studies rely on contrast changes of bundles of DNA on patterned surfaces.<sup>(10, 12, 13)</sup> Individual molecules in the patterns were not resolved in these studies. Yan et al. could resolve the hybridization of individual molecules immobilized on DNA origami tiles.<sup>(14)</sup> A complication is that the tiles are unstable when subjected to annealing, which is needed to improve the specificity of hybridization.<sup>(20)</sup> The stiffness mapping by Husale et al. achieved label-free AFM detection of the hybridization of single molecules on a solid surface for the first time.<sup>(15)</sup> However, the spatial resolution achieved, ~30–50 nm, remains inadequate for single-molecule readout on nanoarrays, in which the probe molecules of a single sequence are localized to spots as small as a few hundred nanometers,<sup>(10)</sup> or for fundamental studies of surface hybridization.<sup>(21)</sup> In this report, we demonstrate that the hybridization of individual DNA molecules can be visualized with an unprecedented imaging resolution (as high as 3 nm) on a novel capture probe surface. The self-assembled monolayer (SAM) surface allows us to switch interactions that can satisfy the contradictory demands for facile hybridization and high-resolution imaging. Nonspecific adsorption was negligible due to the short-range repulsive surface interactions that are present during hybridization. The significantly improved imaging resolution may allow AFM to serve as a readout mechanism for DNA nanoarrays<sup>(10, 13, 22)</sup> and address fundamental questions concerning surface hybridization.

The capture probe surface consists of single-stranded DNA probes that are covalently anchored to a carboxyl-terminated SAM on gold via one of two different methods (Figure 1; see SI for details). The carboxyl terminal groups under a saline Tris-acetate-EDTA (STAE) buffer are ionized at pH 8.0.<sup>(23)</sup> The negative surface charges are expected to lift the tethered probes away from the surface<sup>(24)</sup> and allow them to recognize targets with minimal nonspecific adsorption (Figure 1a). The electrostatic repulsion by the surface, confined to within a few Debye lengths (0.3 nm), is not expected to hinder hybridization significantly. Upon addition of divalent nickel cations, the DNA becomes strongly adsorbed on the surface and can be repeatedly imaged by AFM (Figure 1c). Thus the surface interactions can be switched on demand. Hybridization is carried out when the surface has short-range repulsive interactions with DNA, and imaging is carried out in the presence of Ni<sup>2+</sup> that functions as a salt bridge that pins the DNA to the carboxylate surface.

To test our hypothesis that Ni<sup>2+</sup> may function as salt bridges that immobilize the DNA to the carboxyl SAM surface in a fashion similar to immobilization of DNA on mica,<sup>(7, 25)</sup> we imaged a capture probe surface that had been exposed to 372 bp double-stranded targets possessing a single-stranded 24 nt sticky-end that is complementary to the probes. The chain-like features show that the DNA molecules are effectively immobilized by Ni<sup>2+</sup> with the long axes parallel to the surface (Figure 1e). When the same area was imaged under the STAE buffer, point

protrusions were observed instead (Figure 1f). In order for a structure to be resolved by AFM, it must remain immobile when the tip traverses over the molecule.<sup>(18, 24)</sup> Our previous studies showed that when an anchored DNA molecule is lifted off a weakly interacting surface, only the segment close to the surface anchor contributes to AFM topography, and the rest of the molecule is too mobile to resolve.<sup>(18, 24)</sup> In addition, AFM images acquired under Ni<sup>2+</sup> show that the molecular features rotate around fixed points if the surface is exposed to STAE between the two frames (Figure S1). These results provide clear evidence that the anchored targets became mobile in STAE buffer due to reduced interactions with the negatively charged surface, and that the interactions can be turned on with Ni<sup>2+</sup> to facilitate imaging.

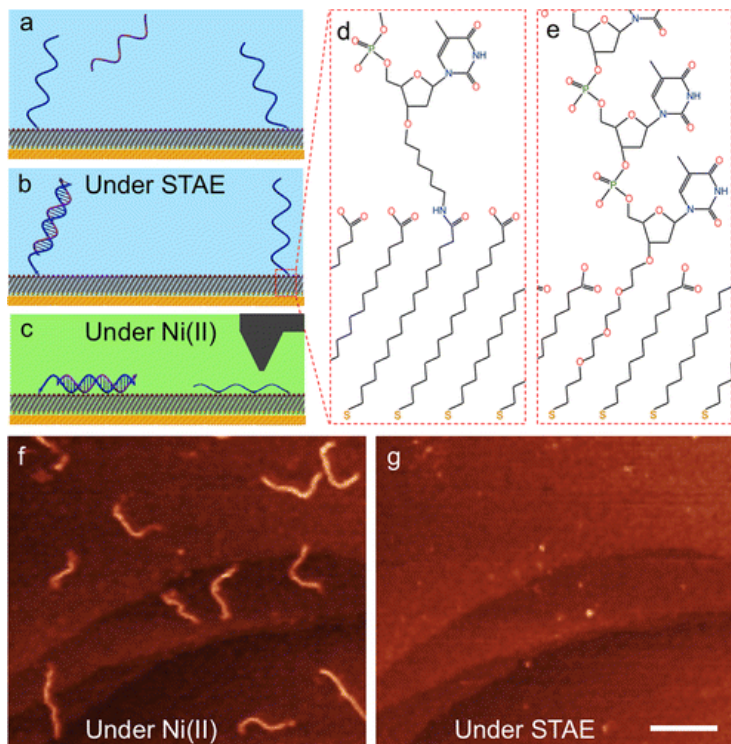


**Figure 1.** Schematic and AFM images of novel capture probe surface. (a) The surface, consisting of DNA probes (blue) covalently anchored to a carboxyl-terminated SAM on gold, is exposed to complementary single-stranded DNA targets (purple) in an STAE buffer. Under this condition, the monolayer is negatively charged, minimizing nonspecific surface interactions. (b) After a predetermined period of time, the surface is rinsed with STAE to remove any unbound targets and (c) placed under a buffer containing Ni<sup>2+</sup>. In the presence of Ni<sup>2+</sup>, the DNA is strongly bound to the surface and can be imaged by the AFM. (d) The probe is covalently coupled to a MHDA monolayer by an amide bond and a six-carbon spacer at its 3'-terminus. (e) In an alternative approach, the probe is attached at the defects of an 11-mercaptoundecanoic acid monolayer by a thiol group and linker at its 3'-terminus. (f) AFM image of captured 396 bp dsDNA targets under a buffer containing Ni<sup>2+</sup>. (g) Image of the same area after switching to STAE buffer. Scale bar is 100 nm.

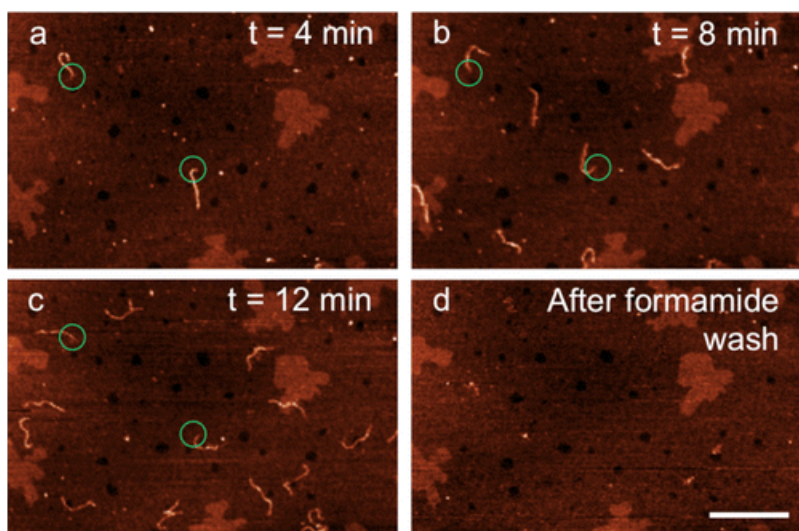


**Figure 2.** Single-molecule AFM detection of hybridization between 24 nt DNA surface probes and solution-phase DNA targets that consist of both a 372 bp double-stranded region and a 24 nt single-stranded segment complementary to the probe. (a–c) At specified times, hybridization was stopped and AFM images were acquired under a buffer containing  $\text{Ni}^{2+}$ . The number of distinct chain-like DNA features increased over time, and the observed chain length is in agreement with the contour length of dsDNA (135 nm). Additionally, the hybridized target molecules were found to rotate around fixed points (green circles) during the hybridization periods. Note that the point features in these images are significantly taller than typical probes and likely represent surface contaminants rather than DNA probes (see SI). (d) Final image shows the same surface after it was exposed to formamide and imaged under the  $\text{Ni}^{2+}$  buffer. All of the targets have dissociated from the surface. Scale bar is 200 nm.

In a further test, the capture probe surface was exposed to an STAE hybridization buffer that contains DNA targets. To track the hybridization process, we periodically stopped the hybridization by rinsing the surface with an STAE buffer and imaged the same area after adding  $\text{Ni}^{2+}$ . The number of the observed targets grew with increasing hybridization time (Figure 2). After the surface with captured targets was exposed to formamide, known to disrupt base-pairing interactions,<sup>(26)</sup> and imaged again under  $\text{Ni}^{2+}$ , the molecular features completely disappeared (Figure 2d). The complete dissociation of targets under formamide, the rotation of molecules around fixed points (green circles in Figure 2), and the absence of captured targets observed on an 16-mercaptohexadecanoic acid (MHDA) SAM prepared without DNA probes (Figure S3) indicate that only the targets that hybridize with the probes remain on the surface after rinsing with STAE. The remarkably low nonspecific adsorption is attributed to the repulsive interactions between DNA and the negatively charged carboxylate surface.

While targets with a double-stranded segment were useful in validating the working principle of our switchable surface, it is important to detect short, single-stranded targets for practical purposes.<sup>(15)</sup> Figure 3a shows that before hybridization, the individual 24mer probes appear as protrusions that are  $\sim 0.6$  nm high. The features were elongated, and the contour lengths were about several nanometers. Short, single-stranded DNAs are more challenging for AFM due to their higher mobility on the surface.<sup>(7)</sup> Even in the few studies that detected single hybridization events with AFM imaging,<sup>(14, 15)</sup> the probes could not be resolved. The effective immobilization

on our SAM surface allows us to resolve probes separated by a distance as small as 3–5 nm, which will help understand how the interprobe interactions impact hybridization. After hybridization with single-stranded 50mer targets, some of the features became  $\sim 1.2$  nm high (Figure 3b). The fraction of the higher features clearly grows with increased hybridization time (Figure 4). Hence, these higher protrusions are attributed to target-probe duplexes, and lower protrusions are probes that remain single-stranded. In different images, the average height of unhybridized probes may vary from 0.6 to 0.8 nm depending on the AFM tip used. Despite the variability, within the same image, hybridized probes display apparent heights that are slightly more than twice the apparent heights of unhybridized probes and hence can be distinguished (Figure 4a).

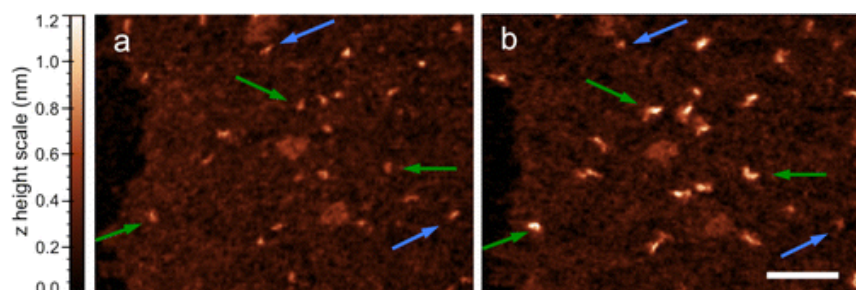


**Figure 3.** AFM images of the same area of the capture probe surface (a) before and (b) after hybridization with 50 nt single-stranded targets. Individual DNA probes initially appear as  $\sim 0.6$  nm tall protrusions. Some of the probes (green arrows) are seen to increase significantly in height to  $\sim 1.2$  nm after exposure to the target DNA, indicating that they have hybridized. Other probes (blue arrows) show little or no height change, indicating that they did not capture a target. Scale bar is 50 nm.

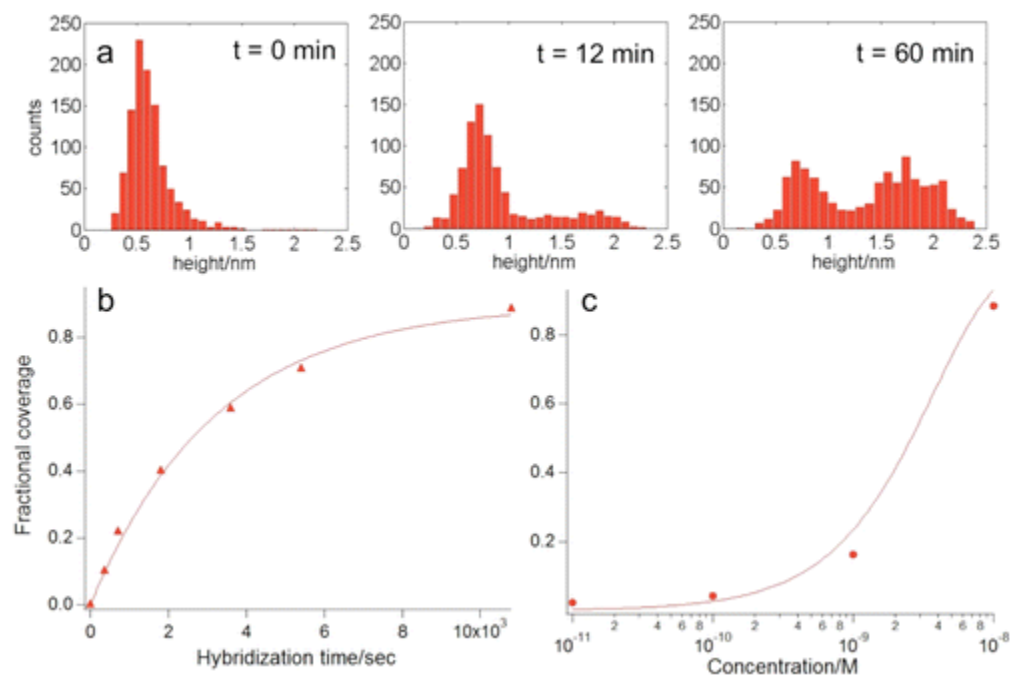
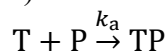


**Figure 4.** (a) Histograms showing topographical heights of single-molecule features in the AFM images at three different hybridization times. (b) Plot of the fractional coverage of DNA probes that have hybridized with a target, i.e., the ratio of the number of hybridized probes to the total

number of probes, as a function of hybridization time. A surface functionalized with 24 nt probes was exposed to a hybridization buffer solution containing 10 nM of 50 nt single-stranded DNA targets. Once the designated time was reached, the surface was rinsed with STAE buffer and imaged by AFM under an aqueous  $\text{Ni}^{2+}$  solution. Note that unlike Figure 2, a fresh surface was used for each data point. Each data point was determined by analyzing multiple images of the same surface, representing at least  $N = 750$  probes; red diamonds are the fractional coverages of hybridized probes,  $\Gamma$ , extracted from the AFM images. The solid line represents a best-fit to an irreversible Langmuir adsorption model,<sup>(6)</sup>  $\Gamma = 1 - e^{-k_a[T]t}$ , where  $t$  is hybridization time,  $[T]$  is target concentration, and  $k_a = (2.47 \pm 0.15) \times 10^4 \text{ M}^{-1} \text{ s}^{-1}$  is the second-order rate constant. (c) Plot of fractional coverage of hybridized probes as a function of target concentration at a fixed hybridization time of  $t = 180$  min. The dots were the observed fractions. The  $\Gamma$  of the solid curve was calculated using the same equation  $\Gamma = 1 - e^{-k_a[T]t}$ , where  $k_a = 2.47 \times 10^4 \text{ M}^{-1} \text{ s}^{-1}$  and  $t = 10800$  s.

Compared to hybridization in solution, surface hybridization typically involves DNA probes at much higher local concentrations.<sup>(1, 5)</sup> Surfaces with very low probe densities are model systems that offer unique insights into intrinsic hybridization kinetics as the interprobe interactions are eliminated and the impact of target transport is lessened.<sup>(1, 5)</sup> Most existing ensemble methods<sup>(1, 3, 5)</sup> do not have the sensitivity to study surface hybridization with probe densities much lower than  $10^{12}/\text{cm}^2$ , a density that still leads to significant interprobe interactions.<sup>(5)</sup> This AFM study allows us to investigate the hybridization kinetics on a surface with negligible interprobe interactions, i.e., with a probe surface density of  $10^{10}$ – $10^{11}/\text{cm}^2$  or even lower. Figure 4 shows that both the time-dependence and target concentration-dependence of hybridization can be described by simple Langmuir kinetics of irreversible adsorption, with each target (T) binding to a single probe (P) to form a target/probe duplex (TP):<sup>(1)</sup>



The rate constant of hybridization,  $k_a$ , on our DNA probe surface is found to be  $(2.47 \pm 0.15) \times 10^4 \text{ M}^{-1} \text{ s}^{-1}$ , which is similar to that observed for thiolated DNA probes on gold,  $\sim 1 \times 10^4 \text{ M}^{-1} \text{ s}^{-1}$ .<sup>(1)</sup> Even on our unoptimized surface, targets at the pM level (Figure 4) can be readily detected. Additional optimization of surface interactions, probe densities,<sup>(1)</sup> and probe design<sup>(20)</sup> should improve target capture and allow detection at the fM level.<sup>(15)</sup> While extracting average quantities from the images helps validate our technique, single-molecule images may provide insight that is not available with existing techniques. We are currently using spatial statistics to quantify the nanoscale environment of individual probe molecules<sup>(27)</sup> and to correlate the local probe crowding with hybridization kinetics.

In summary, switching the interactions between DNA probes and carboxyl-terminated SAMs has allowed facile hybridization with minimal nonspecific adsorption and effective immobilization required for high-resolution AFM imaging. The capture probe surface is simple to prepare, and reproducibly allows AFM to achieve high resolution with the ubiquitous tapping mode and a regular AFM probe. Novel imaging modes<sup>(28)</sup> or smaller AFM cantilevers<sup>(29)</sup> may be used in conjunction with our approach to additionally enhance the resolution and reduce assay time. By enabling single-molecule visualization of closely spaced DNA probes on a surface that can be applied in DNA sensors and microarrays, our system promises to be a powerful tool for understanding how the spatial distribution of probes impacts surface hybridization.<sup>(1, 3-5)</sup> Our

approach will also be valuable to nanoarray detection, which is hampered by the lack of a sensitive, label-free, and quantitative readout mechanism.<sup>(10, 13, 22)</sup>

**Supporting Information.** Details on experimental procedures, description of methods used for AFM image analysis, additional AFM images, and a list of all DNA sequences used. This material is available at <https://doi.org/10.1021/ja401036t>.

**Acknowledgment.** We acknowledge support from UC Merced and NSF (CHE 1048651). We thank Cheetar Lee for supplying the gold microplate substrates.

## References

1. Peterson, A. W.; Heaton, R. J.; Georgiadis, R. M. *Nucleic Acids Res.* **2001**, *29*, 5163– 5168 [Google Scholar](#)
2. Thiel, A.; Frutos, A.; Jordan, C.; Corn, R.; Smith, L. *Anal. Chem.* **1997**, *69*, 4948– 4956 [Google Scholar](#)
3. Ricci, F.; Lai, R. Y.; Heeger, A. J.; Plaxco, K. W.; Sumner, J. *J. Langmuir* **2007**, *23*, 6827– 6834 [Google Scholar](#)
4. Herne, T. M.; Tarlov, M. J. *J. Am. Chem. Soc.* **1997**, *119*, 8916– 8920 [Google Scholar](#)
5. Gong, P.; Levicky, R. *Proc. Natl. Acad. Sci. U.S.A.* **2008**, *105*, 5301– 5306 [Google Scholar](#)
6. Georgiadis, R.; Peterlinz, K.; Peterson, A. J. *Am. Chem. Soc.* **2000**, *122*, 3166– 3173 [Google Scholar](#)
7. Hansma, H. G. *Annu. Rev. Phys. Chem.* **2001**, *52*, 71– 92 [Google Scholar](#)
8. Faas, F. G.; Rieger, B.; van Vliet, L. J.; Cherny, D. I. *Biophys. J.* **2009**, *97*, 1148– 1157 [Google Scholar](#)
9. Wiggins, P. A.; van der Heijden, T.; Moreno-Herrero, F.; Spakowitz, A.; Phillips, R.; Widom, J.; Dekker, C.; Nelson, P. C. *Nat. Nanotechnol.* **2006**, *1*, 137– 141 [Google Scholar](#)
10. Demers, L. M.; Ginger, D. S.; Park, S. J.; Li, Z.; Chung, S. W.; Mirkin, C. *A. Science* **2002**, *296*, 1836– 1838 [Google Scholar](#)
11. Zhou, D. J.; Sinniah, K.; Abell, C.; Rayment, T. *Angew. Chem., Int. Ed.* **2003**, *42*, 4934– 4937 [Google Scholar](#)
12. Liu, M. Z.; Liu, G. Y. *Langmuir* **2005**, *21*, 1972– 1978 [Google Scholar](#)
13. Sinensky, A. K.; Belcher, A. M. *Nat. Nanotechnol.* **2007**, *2*, 653– 659 [Google Scholar](#)
14. Ke, Y.; Lindsay, S.; Chang, Y.; Liu, Y.; Yan, H. *Science* **2008**, *319*, 180– 183 [Google Scholar](#)
15. Husale, S.; Persson, H. H.; Sahin, O. *Nature* **2009**, *462*, 1075– 1078 [Google Scholar](#)

16. Kufer, S. K.; Puchner, E. M.; Gump, H.; Liedl, T.; Gaub, H. *E. Science* **2008**, 319, 594– 596 [Google Scholar](#)
17. Kasas, S.; Thomson, N. H.; Smith, B. L.; Hansma, H. G.; Zhu, X. S.; Guthold, M.; Bustamante, C.; Kool, E. T.; Kashlev, M.; Hansma, P. *K. Biochemistry* **1997**, 36, 461– 468 [Google Scholar](#)
18. Josephs, E. A.; Ye, T. *Nano Lett.* **2012**, 12, 5255– 5261 [Google Scholar](#)
19. Holmberg, M.; Kuhle, A.; Garnaes, J.; Boisen, A. *Ultramicroscopy* **2003**, 97, 257– 261 [Google Scholar](#)
20. Castoldi, M.; Schmidt, S.; Benes, V.; Noerholm, M.; Kulozik, A.; Hentze, M.; Muckenthaler, M. *RNA* **2006**, 12, 913– 920 [Google Scholar](#)
21. Chan, V.; Graves, D. J.; McKenzie, S. E. *Biophys. J.* **1995**, 69, 2243– 2255 [Google Scholar](#)
22. Josephs, E.; Ye, T. *J. Am. Chem. Soc.* **2010**, 132, 10236– 10238 [Google Scholar](#)
23. Vezenov, D.; Noy, A.; Rozsnyai, L.; Lieber, C. J. *Am. Chem. Soc.* **1997**, 119, 2006– 2015 [Google Scholar](#)
24. Josephs, E.; Ye, T. *J. Am. Chem. Soc.* **2012**, 134, 10021– 10030 [Google Scholar](#)
25. Hansma, H. G.; Laney, D. E. *Biophys. J.* **1996**, 70, 1933– 1939 [Google Scholar](#)
26. Mcconaug, B.; Laird, C. D.; McCarthy, B. J. *Biochemistry* **1969**, 8, 3289– 3295 [Google Scholar](#)
27. Josephs, E.; Ye, T. *ACS Nano* **2013**, DOI: 10.1021/nm400659m [Google Scholar](#)
28. Fukuma, T.; Kimura, K.; Kobayashi, K.; Matsushige, K.; Yamada, H. *Rev. Sci. Instrum.* **2005**, 76, 126110 [Google Scholar](#)
29. Leung, C.; Bestembayeva, A.; Thorogate, R.; Stinson, J.; Pyne, A.; Marcovich, C.; Yang, J.; Drechsler, U.; Despont, M.; Jankowski, T.; Tschoepe, M.; Hoogenboom, B. W. *Nano Lett.* **2012**, 12, 3846– 3850 [Google Scholar](#)